

## Review Article

### Single defect centres in diamond: A review

F. Jelezko and J. Wrachtrup\*

3. Physikalisches Institut, Universität Stuttgart, 70550 Stuttgart, Germany

Received 9 February 2006, revised 28 July 2006, accepted 9 August 2006

Published online 11 October 2006

PACS 03.67.Pp, 71.55.–r, 76.30.Mi, 76.70.–r

The nitrogen vacancy and some nickel related defects in diamond can be observed as single quantum systems in diamond by their fluorescence. The fabrication of single colour centres occurs via generation of vacancies or via controlled nitrogen implantation in the case of the nitrogen vacancy (NV) centre. The NV centre shows an electron paramagnetic ground and optically excited state. As a result electron and nuclear magnetic resonance can be carried out on single defects. Due to the localized nature of the electron spin wavefunction hyperfine coupling to nuclei more than one lattice constant away from the defect as dominated by dipolar interaction. As a consequence the coupling to close nuclei leads to a splitting in the spectrum which allows for optically detected electron nuclear double resonance. The contribution discusses the physics of the NV and other defect centre from the perspective of single defect centre spectroscopy.

© 2006 WILEY-VCH Verlag GmbH & Co. KGaA, Weinheim

## 1 Introduction

The ever increasing demand in computational power and data transmission rates has inspired researchers to investigate fundamentally new ways to process and communicate information.

Among others, physicists explored the usefulness of “non-classical”, i.e. quantum mechanical systems in the world of information processing. Spectacular achievements like Shors discovery of the quantum factoring algorithm [1] or the development of quantum secure data communication gave birth to the field of quantum information processing (QIP) [2]. After an initial period where the physical nature of information was explored [3] and how information processing can be carried out by unitary transformation in quantum mechanics, researchers looked out for systems which might be of use as hardware in QIP. From the very beginning it became clear that the restrictions on the hardware of choice are severe, in particular for solid state systems. Hence in the recent past scientists working in the development of nanostructured materials and quantum physics have cooperated on different solid-state systems to define quantum mechanical two-level system, make them robust against decoherence and addressable as individual units. While the feasibility of QIP remains to be shown, *this endeavour will deepen our understanding of quantum mechanics and also marks a new area in material science* which now also has reached diamonds as a potential host material. The usefulness of diamond is based on two properties. First defects in diamond are often characterized by low electron phonon coupling, mostly due to the low density of phonon states i.e. high Debye temperature of the material [4]. Secondly, colour centres in diamond are usually found to be very stable, even under ambient conditions. This makes them unique among all optically active solid-state systems.

\* Corresponding author: e-mail: wrachtrup@physik.uni-stuttgart.de

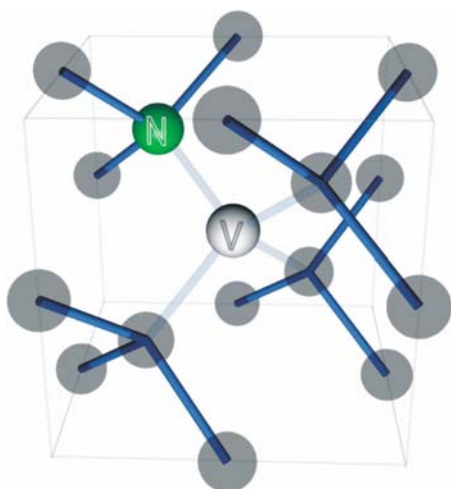


**Fig. 1** (online colour at: [www.pss-a.com](http://www.pss-a.com)) Schematic representation of the nitrogen vacancy (NV) centre structure.

The main goal of QIP is the flexible generation of quantum states from individual two-level systems (qubits). The state of the individual qubits should be changed coherently and the interaction strength among them should be controllable. At the same time, those systems which are discussed for data communication must be optically active which means, that they should show a high oscillator strength for an electric dipole transition between their ground and some optically excited state. Individual ions or ion strings have been applied with great success. Here, currently up to eight ions in a string have been cooled to their ground state, addressed and manipulated individually [5]. Owing to careful construction of the ion trap, decoherence is reduced to a minimum [6]. Landmark experiments, like teleportation of quantum states among ions [7, 8] and first quantum algorithms have been shown in these systems [9, 10].

In solid state physics different types of hardware are discussed for QIP. Because dephasing is fast in most situations in solids only specific systems allow for controlled generation of a quantum state with preservation of phase coherence for a sufficient time. Currently three systems are under discussion. Superconducting systems are either realized as flux or charge quantized individual units [11]. Their strength lies in the long coherence times and meanwhile well established control of quantum states. Main progresses have been achieved with quantum dots as individual quantum systems. Initially the electronic ground as well as excited states (exciton ground state) have been used as definition of qubits [12]. Meanwhile the spin of individual electrons either in a single quantum dot or coupled GaAs quantum dots has been subject to control experiments [13–15]. Because of the presence of paramagnetic nuclear spins, the electron spin is subject to decoherence or a static inhomogeneous frequency distribution. Hence, a further direction of research are Si or SiGe quantum dots where practically no paramagnetic nuclear spins play a significant role. The third system under investigation are phosphorus impurities in silicon [16]. Phosphorus implanted in Si is an electron paramagnetic impurity with a nuclear spin  $I = 1/2$ . The coherence times are known to be long at low temperature. The electron or nuclear spins form a well controllable two-level system. Addressing of individual spins is planned via magnetic field gradients. Major obstacles with respect to nanostructuring of the system have been overcome, while the readout of single spins based on spin-to-charge conversion with consecutive detection of charge state has not been successful yet.

## 2 Colour centres in diamond

There are more than 100 luminescent defects in diamond. A significant fraction has been analysed in detail such that their charge and spin state is known under equilibrium conditions [17]. For this review nitrogen related defects are of particular importance. They are most abundant in diamond since nitrogen is a prominent impurity in the material. Nitrogen is a defect which either exists as a single substitutional impurity or in aggregated form. The single substitutional nitrogen has an infrared local mode of vibration

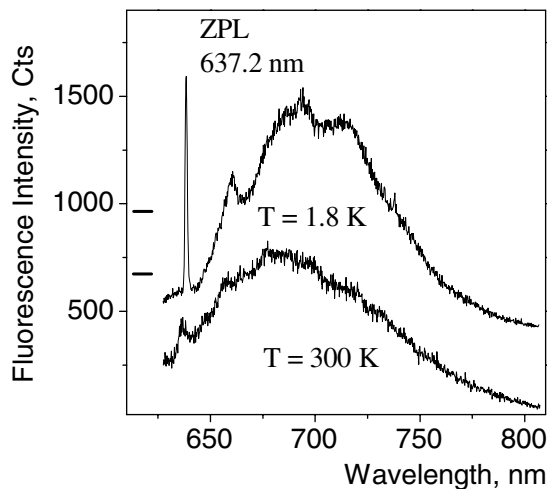


**Fig. 2** Fluorescence emission spectra of single NV centres at room temperature and LHe temperatures. Excitation wavelength was 514 nm.

at  $1344\text{ cm}^{-1}$ . The centre is at a  $C_{3v}$  symmetry site. It is a deep electron donor, probably 1.7 eV below the conduction band edge. There is an EPR signal associated with this defect, called P1, which identifies it to be an electron paramagnetic system with  $S = 1/2$  ground state [17]. Nitrogen aggregates are, most commonly, pairs of neighbouring substitutional atoms, the A aggregates, and groups of four around a vacancy, the B aggregate. All three forms of nitrogen impurities have distinct infrared spectra.

Another defect often found in nitrogen rich type Ib diamond samples after irradiation damage is the nitrogen vacancy defect centre, see Fig. 1. This defect gives rise to a strong absorption at 1.945 eV (637 nm) [18]. At low temperature the absorption is marked by a narrow optical resonance line (zero phonon line) followed by prominent vibronic side bands, see Fig. 2. Electron spin resonance measurements have indicated that the defect has an electron paramagnetic ground state with electron spin angular momentum  $S = 1$  [19]. The zero field splitting parameters were found to be  $D = 2.88\text{ GHz}$  and  $E = 0$  indicating a  $C_{3v}$  symmetry of the electron spin wavefunction. From measurements of the hyperfine coupling constant to the nitrogen nuclear spin and carbon spins in the first coordination shell it was concluded that roughly 70% of the unpaired electron spin density is found at the three nearest neighbour carbon atoms, whereas the spin density at the nitrogen is only 2%. Obviously the electrons spend most of their time at the three carbons next to the vacancy. To explain the triplet ground state mostly a six electron model is invoked which requires the defect to be negatively charged i.e. to be  $NV^-$  [20]. Hole burning experiments and the high radiative recombination rate (lifetime roughly 11 ns [21], quantum yield 0.7) indicate that the optically excited state is also a spin triplet. The width of the spectral holes burned into the inhomogeneous absorption profile were found to be on the order of 50 MHz [22, 23]. Detailed investigation of the excited state dephasing and hole burning have caused speculations as to whether the excited state is subject to a Jan–Teller splitting [24, 25]. From group theoretical arguments it is concluded that the ground state is  $^3A$  and the excited state is of  $^3E$  symmetry. In the  $C_{3v}$  group this state thus comprises two degenerate substrates  $^3E_{x,y}$  with an orthogonal polarization of the optical transition. Photon echo experiments have been interpreted in terms of a Jan Teller splitting of  $40\text{ cm}^{-1}$  among these two states with fast relaxation among them [24]. However, no further experimental evidence is found to support this conclusion. Hole burning experiments showed two mechanisms for spectral hole burning: a permanent one and a transient mechanism with a time scale on the order of ms [23]. This is either interpreted as a spin relaxation mechanism in the ground state or a metastable state in the optical excitation–emission cycle. Indeed it proved difficult to find evidence for this metastable state and also number and energetic position relative to the triplet ground and excited state are still subject of debate. Meanwhile it seems to be clear that at least one singlet state is placed between the two triplet states. As a working hypothesis it should be assumed throughout this article that the optical excitation emission cycle is described by three electronic levels.

### 3 Optical excitation and spin polarization

Given the fact that the NV centre has an electron spin triplet ground state with an optically allowed transition to a  ${}^3E$  spin triplet state one might wonder about the influence of optical excitation on the electron spin properties of the defect. Indeed in initial experiments no electron spin resonance (EPR) signal of the defect was detected except when subject to irradiation in a wavelength range between 450 and 637 nm [19]. Later on it became clear that in fact there is an EPR signal even in the absence of light, yet the signal strength is considerably enhanced upon illumination [26]. EPR lines showed either absorptive or emissive line shapes depending on the spectral position. This indicates that only specific spin sub-levels are affected by optical excitation [27]. In general a  $S = 1$  electron spin system is described by a spin Hamiltonian of the following form:  $H = g_e \beta \mathbf{B} \hat{S} + \hat{S} D \hat{S}$ . Here  $g_e$  is the electronic  $g$ -factor ( $g = 2.0028 \pm 0.0003$ );  $B_0$  is the external magnetic field and  $D$  is the zero field splitting tensor. This tensor comprises the anisotropic dipolar interaction of the two electron spins forming the triplet state averaged over their wave function. The tensor is traceless and thus characterized by two parameters,  $D$  and  $E$  as already mentioned above. The zero field splitting causes a lifting of the degeneracy of the spin sub-levels  $m_s = \pm 1, 0$  even in the absence of an external magnetic field. Those zero field spin wave functions  $T_{x,y,z}$  do not diagonalize the full high-field Hamiltonian  $H$  but are related to these functions by

$$T_x = \frac{1}{\sqrt{2}} |\beta_1 \beta_2 - \alpha_1 \alpha_2\rangle = \frac{1}{\sqrt{2}} |T_{-1} - T_{+2}\rangle,$$

$$T_y = \frac{i}{\sqrt{2}} |\beta_1 \beta_2 + \alpha_1 \alpha_2\rangle = \frac{1}{\sqrt{2}} |T_{-1} + T_{+1}\rangle,$$

$$T_z = \frac{1}{\sqrt{2}} |\alpha_1 \beta_2 + \beta_1 \alpha_2\rangle = |T_0\rangle.$$

The expectation value of  $S_z$  for all three wave functions  $\langle T_{x,y,z} | S_z | T_{x,y,z} \rangle$  is zero. Hence there is no magnetization in zero external field. There are different ways to account for the spin polarization process in an excitation scheme involving spin triplets. To first order optical excitation is a spin state conserving process. However spin-orbit (LS) coupling might allow for a spin state change in the course of optical excitation. Cross relaxation processes on the other hand might cause a strong spin polarization as it is observed in the optical excitation of various systems, like e.g. GaAs. However, optical spectroscopy and in particular hole burning data gave little evidence for non spin conserving excitation processes in the NV centre. In two laser hole burning experiments data have been interpreted by assuming different zero field splitting parameters in ground and excited state ( $D^{\text{exc}} \approx 2 \text{ GHz}$ ,  $E^{\text{exc}} \approx 0.8 \text{ GHz}$ ) by an otherwise spin state preserving optical excitation process [28]. Indeed this is confirmed by later attempts to generate ground state spin coherence via Raman process [29], which only proves to be possible when ground state spin sublevels are brought close to anticrossing by an external magnetic field. Another spin polarising mechanism involves a further electronic state in the optical excitation and emission cycle [30, 31]. Though being weak, LS coupling might be strong enough to induce intersystem crossing to states with different spin symmetry, e.g. a singlet state. Indeed the relative position of the  ${}^1A$  singlet state with respect to the two triplet states has been subject of intense debate. Intersystem crossing is driven by LS induced mixing of singlet character into triplet states. Due to the lack of any emission from the  ${}^1A$  state or noticeable absorption to other states, no direct evidence for this state is at hand up to now. However, the kinetics of photo emission from single NV centres strongly suggests the presence of a metastable state in the excitation emission cycle of the state. As described below the intersystem crossing rates from the excited triplet state to the singlet state are found to be drastically different, whereas the relaxation to the  ${}^3A$  state might not depend on the spin substate. This provides the required optical excitation dependent relaxation mechanism. Bulk as well as single centre experiments show that predominantly the  $m_s = 0$  ( $T_z$ ) sublevel in the spin ground state is populated. The polarization in this state is on the order of 80% or higher [27].

#### 4 Spin properties of the NV centre

Because of its paramagnetic spin ground and excited state the NV centre has been the target of numerous investigations regarding its magneto-optical properties. Pioneering work has been carried out in the groups of Manson [32–36], Glasbeek [37–39] and Rand [26, 40, 41].

The hyperfine and fine structure splitting of the NV ground state has been used to measure the Autler–Townes splitting induced by a strong pump field in a three level system. Level anticrossing among the  $m_s = 0$  and  $m_s = -1$  allows for an accurate measurement of the hyperfine coupling constant for the nitrogen nucleus, yielding an axially symmetric hyperfine coupling tensor with  $A_{\parallel} = 2.3$  MHz and  $A_{\perp} = 2.1$  MHz [42, 43]. The quadrupole coupling constant  $P = 5.04$  MHz. Because of its convenient access to various transitions in the optical, microwave and radiofrequency domain the NV centre has been used as a model system to study the interaction between matter and radiation in the linear and non-linear regime. An interesting set of experiments concerns electromagnetically induced transparency in a  $\Lambda$ -type level scheme. The action of a strong pump pulse on one transition in this energy level scheme renders the system transparent for radiation resonant with another transitions. Experiments have been carried out in the microwave frequency domain [44] as well as for optical transitions among the  $^3A$  ground state and the  $^3E$  excited state [29]. Here two electron spin sublevels are brought into near level anticrossing such that an effective three level system is generated with one excited state spin sublevel and two allowed optical transitions. A 17% increase in transmission is detected for a suitably tuned probe beam.

While relatively much work has been done on vacancy and nitrogen related impurities comparatively little is known about defects comprising heavy elements. For many years it was difficult to incorporate heavy elements as impurities into the diamond lattice. Only six elements have been identified as bonding to the diamond lattice, namely nitrogen, boron, nickel, silicon, hydrogen and cobalt. Attempts to use ion implantation techniques for incorporation of transition metal ions were unsuccessful. This might be due to the large size of the ions and the small lattice parameters of diamond together with the metastability of the diamond lattice at ambient pressure. Recent developments in crystal growth and thin film technology have made it possible to incorporate various dopants into the diamond lattice during growth. This has enabled studies of nickel defects [45, 46]. Depending on the annealing conditions Ni can form clusters with various vacancies and nitrogen atoms in nearest neighbour sites. Different Ni related centres are listed with NE as a prefix and numbers to identify individual entities. The structure and chemical compo-

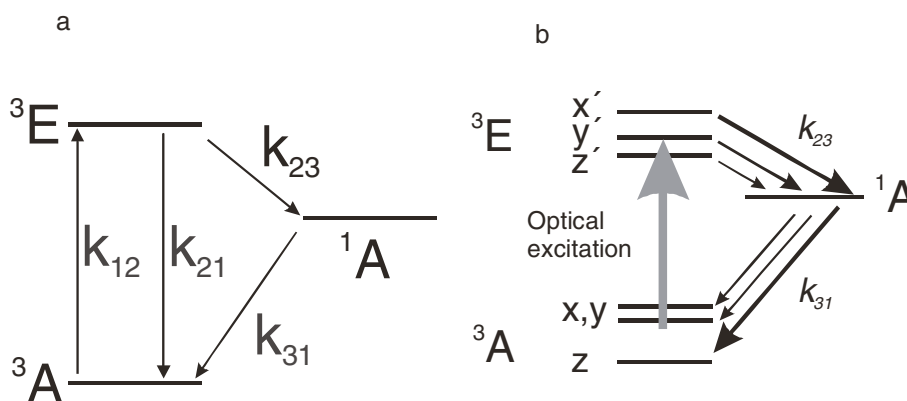


**Fig. 3** a) Three level scheme describing the optical excitation and emission cycle of single NV centres.  $^3A$  and  $^3E$  are the triplet ground and excited state.  $^1A$  is a metastable singlet state. No information is at hand presently about the number and relative position of singlet levels. The arrows and  $k_{ij}$  denote the rates of transition among the various states. b) More detailed energy level scheme differentiating between triplet sublevels in the  $^3A$  and  $^3E$  state.

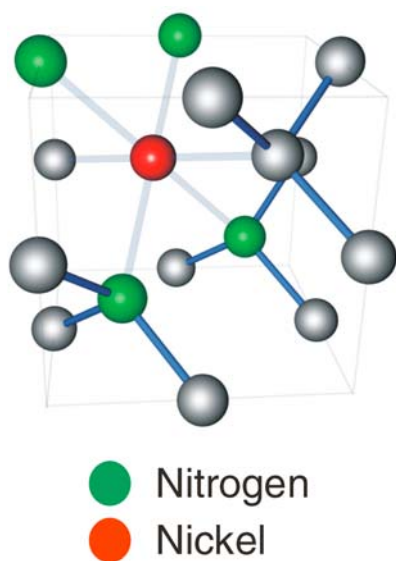


**Fig. 4** (online colour at: [www.pss-a.com](http://www.pss-a.com)) Structure of the NE8 centre.

sition of defects have mostly been identified by EPR on the basis of the hyperfine coupling to nitrogen nuclei [46]. A particularly rich hyperfine structure has been identified for the NE8 centre.

Analysis of the angular dependence of the EPR spectrum for the NE8 centre showed that this centre has electronic spin  $S = 1/2$  and a  $g$ -value typical of a  $d$ -ion with more than half filled  $d$ -shell. The NE8 centre has been found not only in HPHT synthetic diamonds but also in natural diamonds which contain the nickel-nitrogen centres NE1 to NE3 [46]. The structure of the centre is shown in Fig. 4. It comprises 4 substitutional nitrogen atoms and an interstitial Ni impurity. The EPR signature of the system has been correlated to an optical zero phonon transition at around 794 nm. The relative integral intensity of the zero phonon line and the vibronic side band at room temperature is 0.7 (Debye–Waller factor) [47]. The fluorescence emission statistics of single NE8 emitters shows a decay to a yet unidentified metastable state with a rate of 6 MHz.

## 5 Single defect centre experiments

Experiments on single quantum systems in solids have brought about a considerable improvement in the understanding of the dynamics and energetic structure of the respective materials. In addition a number of quantum optical phenomena, especially when light–matter coupling is concerned, have been investigated. As opposed to atomic systems on which first experiments on single quantum systems are well established, similar experiments with impurity atoms in solids remain challenging. Single quantum systems in solids usually strongly interact with their environment. This has technical as well as physical consequences. First of all single solid state quantum systems are embedded in an environment which, for example, scatters excitation light. Given a diffraction limited focal volume usually the number of matrix atoms exceed those of the quantum systems by  $10^6$ – $10^8$ . This puts an upper limit on the impurity content of the matrix or on the efficiency of inelastic scattering processes like e.g. Raman scattering from the matrix. Various systems like single hydrocarbon molecules, proteins, quantum dots and defect centres have been analysed [48]. Except for some experiments on surface enhanced Raman scattering the technique usually relies on fluorescence emission. In this technique an excitation laser in resonance with a strongly allowed optical transition of the system is used to populate the optically excited state (e.g. the  $^3E$  state for the NV centre), see Fig. 3a. Depending on the fluorescence emission quantum yield the system either decays via fluorescence emission or non-radiatively, e.g. via inter-system-crossing to a metastable

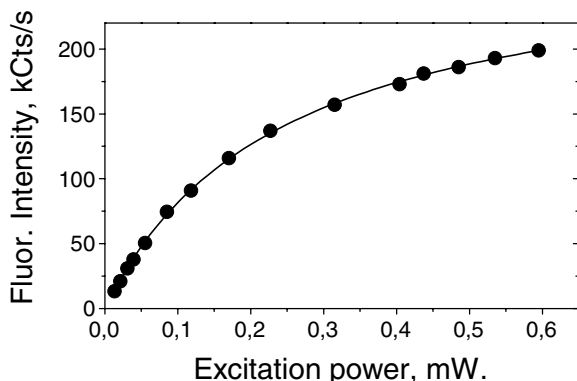


**Fig. 5** Saturation curve of the fluorescence intensity of a single NV centre at  $T = 300$  K. Excitation wavelength is 514 nm. The power is measured at the objective entrance.

state ( $^1A$  in the case of the NV). The maximum numbers of photons emitted are given when the optical transition is saturated. In this case the maximum fluorescence intensity is given as

$$I_{\max} = \frac{k_{31}(k_{21} + k_{23})\Phi_F}{2k_{31} + k_{23}}.$$

Here  $k_{31}$  is the relaxation rate from the metastable to the ground state and  $k_{21}$  is the decay rate of the optically excited state,  $k_{23}$  is the decay rate to the metastable state and  $\Phi_F$  marks the fluorescence quantum yield. For the NV centre  $I_{\max}$  is about  $10^7$  photon/s.  $I_{\max}$  critically depends on a number of parameters. First of all the fluorescence quantum yield limits the maximum emission. A good example to illustrate this is the GR1 centre, the neutral vacancy defect in diamond. The overall lifetime of the excited state for this defect is 1 ns at room temperature. However, the radiative lifetime is on the order of 100 ns. Hence  $\Phi_F$  is on the order of 0.01. Given the usual values for  $k_{21}$  and  $k_{31}$  this yields an  $I_{\max}$  which is too low to allow for detecting single GR1 centres with current technology. Figure 5 shows the saturation curve of a single NV defect. Indeed the maximum observable emission rate from the NV centre is around  $10^5$  photons/s which corresponds well to the value estimated above, if we assume a detection efficiency of 0.01. Single NV centres can be observed by standard confocal fluorescence microscopy in type Ib diamond. In confocal microscopy a laser beam is focussed onto a diffraction limited spot in the diamond sample and the fluorescence is collected from that spot. Hence the focal probe volume is diffraction limited with a volume of roughly  $1 \mu\text{m}^3$ . In order to be able to detect single centres it is thus important to control the density of defects. For the NV centre this is done by varying the number of vacancies created in the sample by e.g. choosing an appropriate dose of electron irradiation. Hence the number of NV centres depends on the number of vacancies created and the number of nitrogen atoms in the sample. Figure 7 shows an image of a diamond sample where the number of defects in the sample is low enough to detect the fluorescence from single colour centres [49]. As expected the image shows diffraction limited spots. From the image alone it cannot be concluded whether the fluorescence stems from a single quantum system or from aggregates of defects. To determine the number of independent emitters in the focal volume the emission statistics of the NV centre fluorescence can be used [50–52]. The fluorescence photon number statistics of a single quantum mechanical two-level system deviates from a classical Poissonian distribution. If one records the fluorescence intensity autocorrelation function  $g^2(\tau) = \frac{\langle I(t)I(t+\tau) \rangle}{\langle I(t) \rangle^2}$

for short time  $\tau$  one finds  $g^2(0) = 0$  if the emission stems from a single defect centre (see Fig. 6). This is due to the fact that the defect has to be excited first before it can emit a single photon. Hence a single defect never emits two fluorescence photons simultaneously, in contrast to the case when a number of independent emitters are excited at random. If one adopts the three level scheme from Fig. 3a, rate equations for temporal changes of populations in the three levels can be set up. The equations are solved by

$$g^{(2)}(\tau) = 1 - (K + 1)e^{-k_1\tau} + Ke^{-k_2\tau},$$

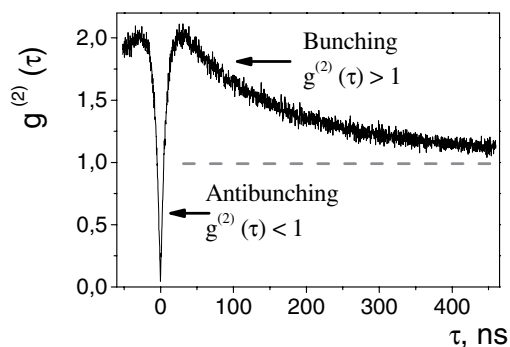


**Fig. 6** Fluorescence intensity autocorrelation function of a single NV defect at room temperature.

with rates  $k_{1,2} = -\frac{1}{2}P \pm \sqrt{\frac{1}{4}P^2 - Q}$ . Here  $P = k_{21} + k_{12} + k_{23} + k_{31}$  and  $Q = k_{31}(k_{21} + k_{12}) + k_{23}(k_{31} + k_{12})$  with

$$K = \frac{k_2 + k_{31} - k_{12} \frac{k_{23}}{k_{31}}}{k_1 - k_2}.$$

This function reproduces the dip in the correlation function  $g^2(\tau)$  for  $\tau \rightarrow 0$  shown in Fig. 6, which indicates that the light detected originates from a single NV. The slope of the curve around  $\tau = 0$  is determined by the pumping power of the laser  $k_{12}$  and the decay rate  $k_{21}$ . For larger times  $\tau$  a decay of the correlation function becomes visible. This decay marks the ISC process from the excited triplet  $^3E$  to the metastable singlet state  $^1A$ . Besides the spin quantum jumps detected at low temperature the photon statistics measurements are the best indication for detection of single centres. It should be noted that the radiative decay time depends on the refractive index of the surrounding medium as  $1/n_{\text{medium}}$ . Because  $n_{\text{medium}}$  of diamond is 2.4 the decay time should increase significantly if the refractive index of the surrounding is reduced. This is indeed observed for NV centres in diamond nanocrystals [51]. It should be

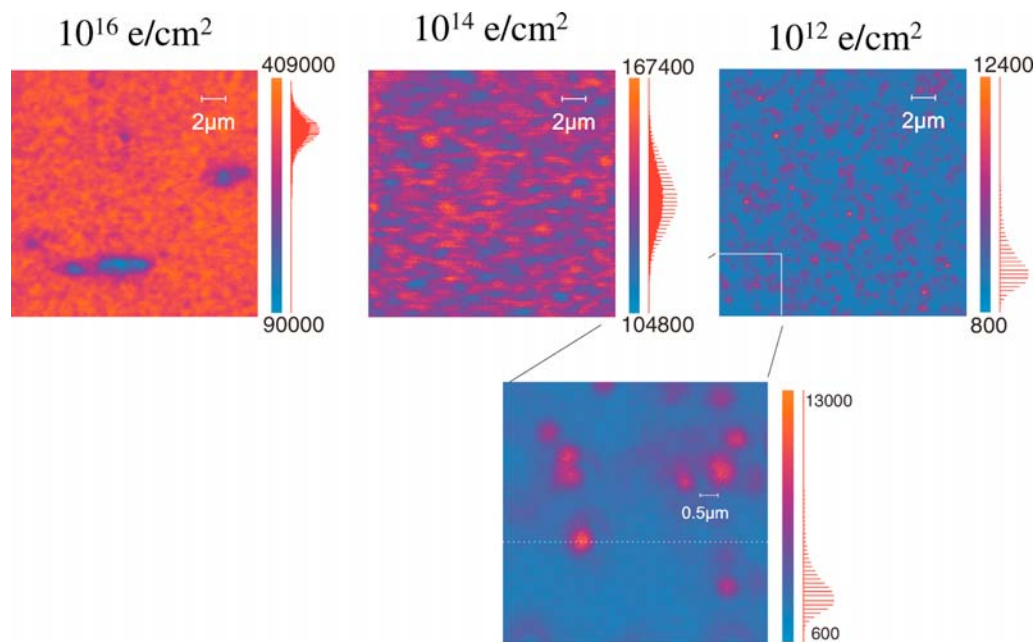


**Fig. 7** (online colour at: [www.pss-a.com](http://www.pss-a.com)) Confocal fluorescence image of various diamond samples with different electron irradiation dosages.



noted, that owing to their stability single defect centres in diamond are prime candidates for single photon sources under ambient conditions. Such sources are important for linear optics quantum computing and quantum cryptography. Indeed quantum key distribution has been successful with fluorescence emission from single defect centres [53].

A major figure of merit for single photon sources is the signal to background ratio, given (e.g.) by the amplitude of the correlation function at  $\tau = 0$ . This ratio should be as high as possible to ensure that a single bit of information is encoded in a single photon only. The NV centre has a broad emission range which does not allow efficient filtering of background signals. This is in sharp contrast to the NE8 defect which shows a very narrow, only 1.2 nm wide spectrum. As a consequence the NE8 emission can be filtered out efficiently [47]. The correlation function resembles the one from the NV centre. Indeed the photophysical parameters of the NV and NE8 are similar, yet under comparable experimental conditions the NE8 shows an order of magnitude improvement in signal-to-background ratio because of the narrower emission range.

Besides application in single photon generation, photon statistical measurements also allow to derive conclusions on photoionization and photochromism of single defects. Most notably the NV centre is speculated to exist in two charge forms, the negatively charged NV with zero phonon absorption at 637 nm and the neutral form  $\text{NV}^0$  with absorption around 575 nm [20, 54]. Although evidence existed that both absorption lines stem from the same defect no direct charge interconversion has been shown in bulk experiments. The best example for a spectroscopically resolved charge transfer in diamond is the vacancy, which exists in two stable charge states. In order to observe the charge transfer from NV to  $\text{NV}^0$  photon statistical measurements similar to the ones described have been carried out, except for a splitting of photons depending on the emission wavelength [55]. This two channel set up allows to detect the emission of  $\text{NV}^0$  in one and NV in another detector arm. Figure 8 shows the experimental result. For delay time  $\tau = 0$ ,  $g^2(\tau)$  shows a dip, indicating the sub-Poissonian statistics of the light emitted. It should

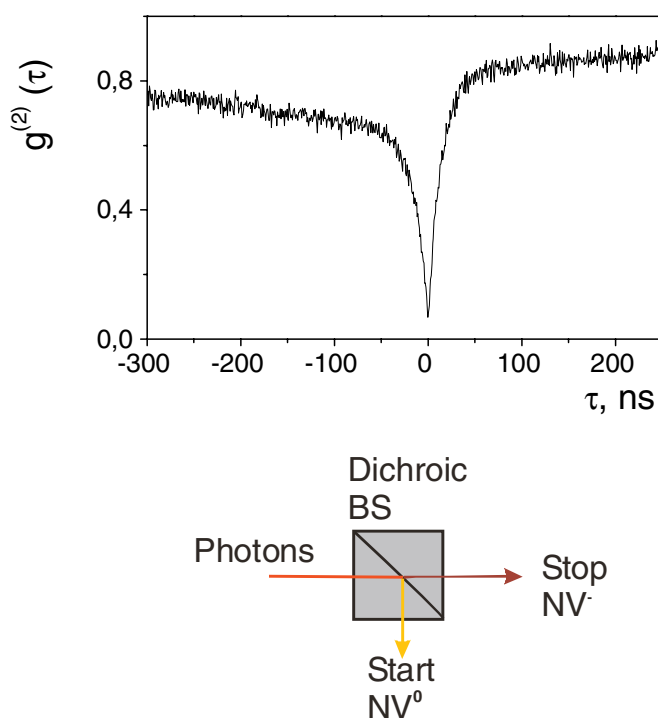


**Fig. 8** (online colour at: [www.pss-a.com](http://www.pss-a.com)) Fluorescence cross correlation function between the  $\text{NV}^0$  and NV emission of a single defect.

be noted, that for recording Fig. 8.  $g^2(\tau)$  has been detected in a cross correlation type of measurement between  $NV^0$  and NV photons. The data acquisition was started by detection of a NV and stopped by the detection of a  $NV^0$  photon. The coincidence rate ( $\tau = 0$ ) in Fig. 8 is zero. Hence it must be concluded that there is a continuous interconversion between the two spectral positions. Detailed time resolved experiments show that switching from  $NV^0$  to NV is photoinduced whereas the reverse process NV to  $NV^0$  occurs under dark conditions with a time constant between 0.3 and 3.6  $\mu$ s.

## 6 Spin physics of single defects

The controlled generation of quantum states from individual quantum objects is a current research topic which receives considerable interest during the last decade. In part this is motivated by possible applications in quantum information processing. On the other hand, the simulation of quantum systems itself, for example to investigate the physics of quantum phase transitions, is of interest. Basically the control of a wave function of a collective quantum state requires control over the quantum state of interacting

qubits:  $\psi = \sum_i^N a_i |\alpha_i\rangle$ . The evolution of  $\psi$  is subject to unitary transformations:  $\psi' = U\psi$ . In general it is

necessary to be able to manipulate coherently each individual qubit and control the strength of interaction among them. This puts certain restrictions on the system parameters. To allow for nontrivial unitary operations  $U$  a certain phase coherence time together with interaction strength and speed of operation is required. While the interaction strength and control speed of individual qubits are limited by technical means, the dephasing times in solids are usually short. Spins are certainly among the most promising systems owing to long coherence times together with availability of fast control of individual qubits and relatively strong spin–spin coupling. Although such robust control of spin states plus adjustment of spin–spin interactions are common practice in electron and nuclear magnetic resonance, the measurement of single spin states is a fierce experimental challenge. Only a few solid state systems currently allow for single spin state detection. Most notably single spin state measurements have been successful in III–V quantum dots and in  $P$  centre defects in silicon single electron transistor (SET) structures. A system where single spin control and state measurement are well developed is the NV centre using optical technique. It is remarkable that for spins associated with defects in diamond, phase memory times can be long even under ambient conditions. As an example the electron spin lattice time is reported to be 1.8 ms at  $T = 300$  K. The long dephasing times are attributed to the low phonon density of states in diamond even at room temperature. In the NV centre the spin state is detected via fluorescence. As discussed above the fluorescence intensity  $I_{\max}$  depends on the spin state via the ISC rate  $k_{23}$ . Upon changing the spin state this rate is changed from some kHz by more than three orders of magnitude towards some MHz. Given the other parameters this results in a change of roughly 30% of  $I_{\max}$ . Taking into account the photon shot noise and an average  $I_{\max}$  of  $10^5$  photocounts per second, this change in fluorescence intensity can be detected with some ms averaging time. Figure 9 shows an example of an optically detected magnetic resonance (ODMR) spectrum of a single NV defect. The spin Hamiltonian describing the spectrum is

$$H = g_e \beta_e \mathbf{B}_0 \mathbf{S} + \mathbf{SAI} - g_N \beta_N \mathbf{IB}.$$

The spectra have been taken without an external  $B_0$  field. Hence only the fine structure ( $SDS$ ) and hyperfine term  $SAI$  need to be considered. As mentioned above, due to the  $C_{3v}$  symmetry two of the three spin sublevels are degenerated ( $E = 0$ ). Hence, only a single ODMR line is seen in the spectrum. Upon application of a  $B_0$  field the two degenerated levels split and two lines become visible. The hyperfine coupling to the  $^{14}\text{N}$  nucleus is not resolved in these spectra because of the large optical pumping rate used [56]. Since the hyperfine and quadrupole coupling constants are 2 and 5 MHz only, the corresponding splitting are easily masked by the homogeneous transition line width. For the NV centre this line width depends on the optical excitation intensity, since at least one of the levels is optically excited to the  $^3E$

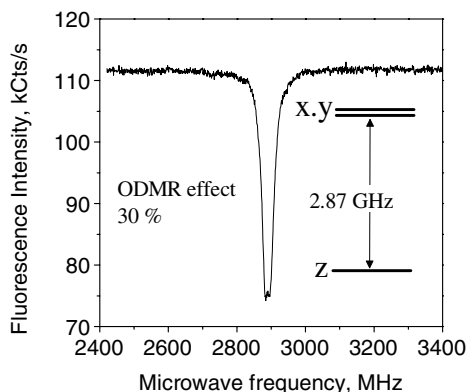


**Fig. 9** Optically detected magnetic resonance (ODMR) spectrum of a single defect. The spectrum has been recorded at room temperature with 514 nm irradiation without an external  $B_0$ .

state. Since the optical Rabi frequency easily achieves some MHz, the line width correspondingly gets broad. As a consequence for low excitation power the hyperfine and quadruple structure gets resolved, as shown in Fig. 10a. The hyperfine structure in Fig. 10 has been analysed in detail [56] and corresponds to the known value of the hyperfine and quadruple coupling of the  $^{14}\text{N}$  nucleus of the NV centre. It should be noted that these spectra provide an opportunity to verify the mechanism by which the defect has been generated. There are two mechanisms by which NV centres can be created in diamonds. First, vacancies are generated and the intrinsic nitrogen present in the material is used to create NV centres. Alternatively, the nitrogen atoms are implanted in nitrogen-free diamond and the vacancies which are generated during the implantation form NV defects. To ensure that a defect centre originates from an implanted nitrogen,  $^{15}\text{N}$  isotope, which has a natural abundance of only 0.1% and is a  $I = 1/2$  nucleus, can be used. A corresponding ODMR spectrum is shown in Fig. 10a and is clearly different from the  $^{14}\text{N}$  case. A completely different set of hyperfine coupling parameters is measured when a  $^{13}\text{C}$  nucleus is found in the shell of first nearest neighbours around the vacancy. Because of the much higher spin density of the electron at these carbon positions the measured coupling parameter is around 130 MHz (see Fig. 10b).

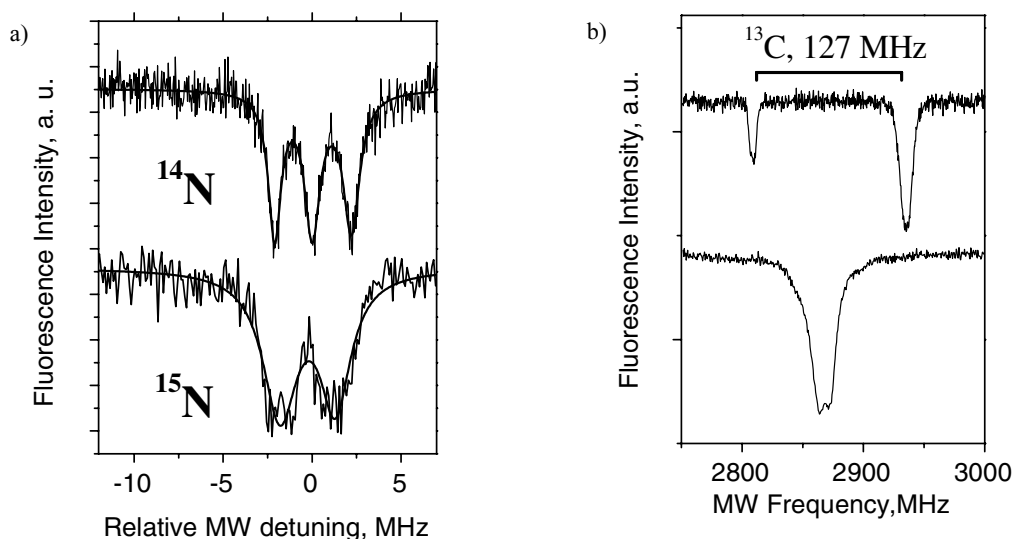


**Fig. 10** ODMR spectra with resolved  $^{14}\text{N}$  and  $^{15}\text{N}$  hyperfine structure (a) and  $^{13}\text{C}$  hyperfine structure (b). The spectra have been acquired at room temperature without the application of an external magnetic field.

## 7 Coherence and single spin states

The generation of a coherent state superposition is achieved by a short microwave pulse in resonance with the transition in Fig. 9 or one of the transitions in Fig. 10. In order to generate a state superposition with arbitrary expansion coefficients of the two eigenstates e.g.  $|\alpha\rangle$  and  $|\beta\rangle$  one uses microwave pulses of variable length, such that  $\psi(t) = \sin \Omega_{\text{MW}} t |m_s = 0\rangle + \cos \Omega_{\text{MW}} t |m_s \pm 1\rangle$  (here  $\Omega_{\text{MW}}$  is the microwave Rabi frequency). Depending on the magnitude of  $\cos^2 \Omega_{\text{MW}} t$  the fluorescence will change. Hence when plotting the fluorescence intensity as a function of pulse length a periodical variation of the fluorescence is seen (see Fig. 11). The frequency of these oscillations (Rabi nutations) depends linearly on the MW field amplitude, as can be seen in Fig. 11 [57]. Rabi frequencies of up to 140 MHz have been achieved with miniaturized coupling loops or wire structures. For the nutation curve in Fig. 11 a decay of the amplitude is expected. The corresponding decay constant is related to the dephasing time  $T_2$  but not equivalent to  $T_2$ . Rather  $T_2$  has to be measured in the absence of any microwave field. This is achieved by the application of a Hahn echo sequence. In this pulse sequence all inhomogeneous distribution of resonance frequencies are refocused while fluctuation of transition frequency or random phase jumps cause an echo decay upon increasing the time between pulses. Figure 12 shows an example of a Hahn echo train with variable delay. An echo decay is visible which can be fitted with a monoexponential decay time of 350  $\mu\text{s}$ . The chief cause for dephasing in diamond are electron paramagnetic impurities in the lattice [58]. These impurities show dipolar coupling to the NV centre and hence may undergo energy conserving spin flip-flop processes with the NV spin. These processes result in a loss of phase memory of the NV spin. It has been demonstrated, that the NV centre  $T_2$  time depends on the concentration of impurities in the lattice and the dephasing time was shown to decrease up to some hundred ns for nitrogen-rich diamond.

In defects which do show a hyperfine coupling to a  $^{13}\text{C}$  nucleus in addition to electron spin also nuclear spin nutations can be detected [59]. Because nuclear spin wave functions do not couple to the optical transition outside of level anticrossing, all changes in nuclear spin wave function must be mapped into the electron spin states to be detectable. A single electron plus nuclear spin system is described by a four level system. To first order only electron spin resonance transitions with  $\Delta m_s = 1$  and  $\Delta m_i = 0$  are allowed, indicated by the two arrows in Fig. 13. In order to drive nuclear magnetic resonance transitions, radio frequency has to be irradiated at transition energy between level 1 and 2 (or level 3 and 4). For the 1–2 transition this corresponds to the hyperfine splitting observed in Fig. 10b.

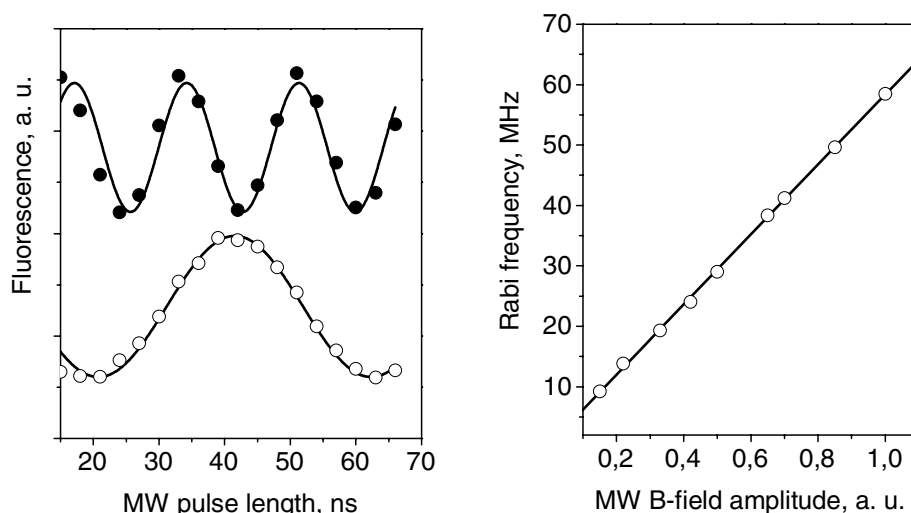


**Fig. 11** Optically detected Rabi nutations of a single NV electron spin. The points represent experimental data and the line is a fit with a  $\cos^2 \Omega t$  function, where  $\Omega$  is the spin Rabi frequency. Figure on right: Dependence of Rabi frequency on MW field amplitude. The solid line represents a linear fit.

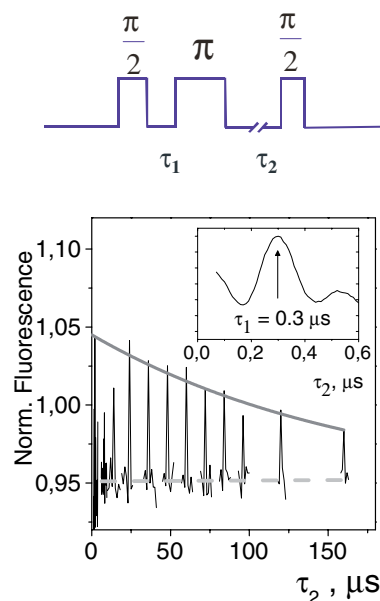


**Fig. 12** (online colour at: [www.pss-a.com](http://www.pss-a.com)) Hahn echo trace of a single spin. The upper part of the figure shows the microwave pulse sequence used. The lower part depicts experimental data. The inset shows the Hahn echo itself. The main figure demonstrates the Hahn echo decay as a function of  $\tau_1 = \tau_2$ . Printed are the individual echoes at different delay times together with a fitted decay curve of the amplitude.

$^{13}\text{C}$  nuclear relaxation times in diamond vary between 1.4 and 36 h. The  $T_2$  time can be estimated from the width of  $^{13}\text{C}$  NMR spectra to be on the order of ms for those nuclei that are not detuned from the dipolar nuclear spin bath. Hence, nuclear spin states should allow for coherent state preparation. To observe nuclear spin transients a microwave-radio frequency double resonance experiment has been carried out. The experiment comprises  $\pi$  pulses separated by time  $\tau$ . During this time interval a radio frequency pulse of variable length in resonance with e.g. the 2–1 transition is applied. The strength of the EPR signal is measured on the 3–1 transition. Figure 13 shows an example of a nuclear transient measured in this way. The amplitude of the oscillations corresponds to the amplitude of the ODMR signal itself, i.e. 30% of the fluorescence intensity. The approach corresponds to the well known electron-nuclear double resonance experiments. With two spins at hand it is possible to carry out basic quantum computation experiments like, e.g. the conditional not gate (CNOT). It can be shown, that two gate operations are sufficient to perform all operations necessary for full quantum computation. These two gates are the single quantum bit NOT gate, which corresponds to an inversion of the bit value and the CNOT gate which is the inversion of one bit conditioned on the value of a second bit. In this nomenclature a single qubit corresponds to a single spin with either of the two eigenvalues  $|0\rangle$  or  $|1\rangle$  (spin-up or spin-down). A CNOT gate would flip, e.g. the electron spin depending on the state of the nuclear spin. Such a scenario can be easily realized in a situation shown in Fig. 13, i.e. in a 4 level system with coherent control over (at least) two transitions. For example the nuclear spin will be inverted only by RF irradiation in resonance with the 1–2 transition when the electron is in spin-up configuration, i.e. in state 1. A simplified version of the CNOT gate is the CROT transformation. The two operations are identical to each other except for a phase factor which can be achieved by a rotation around the z-axis. The CROT itself is only a  $\pi$  pulse. The action of the pulse only corresponds to an ideal gate in the limit of infinitely narrow spectral lines, i.e. long  $T_2$  and rectangular microwave pulses. Under realistic conditions this is not the case. Performing more complex quantum information operations requires a certain precision of operations. Hence, it is useful to control the quality of gates. The result of such a gate tomography experiment is shown in Fig. 14. Here a pulse has been applied to transition 1–2 for various initial conditions, i.e. the system being in state 1, 3, 4 before start of the  $\pi$  pulse. For an ideal situation one would expect the system to end up in state 2 when it started in 1 with the only non-zero matrix element of the  $4 \times 4$  density matrix describing the system to be  $\rho_{22}$  after the pulse. However because of the finite dephasing time  $T_2$

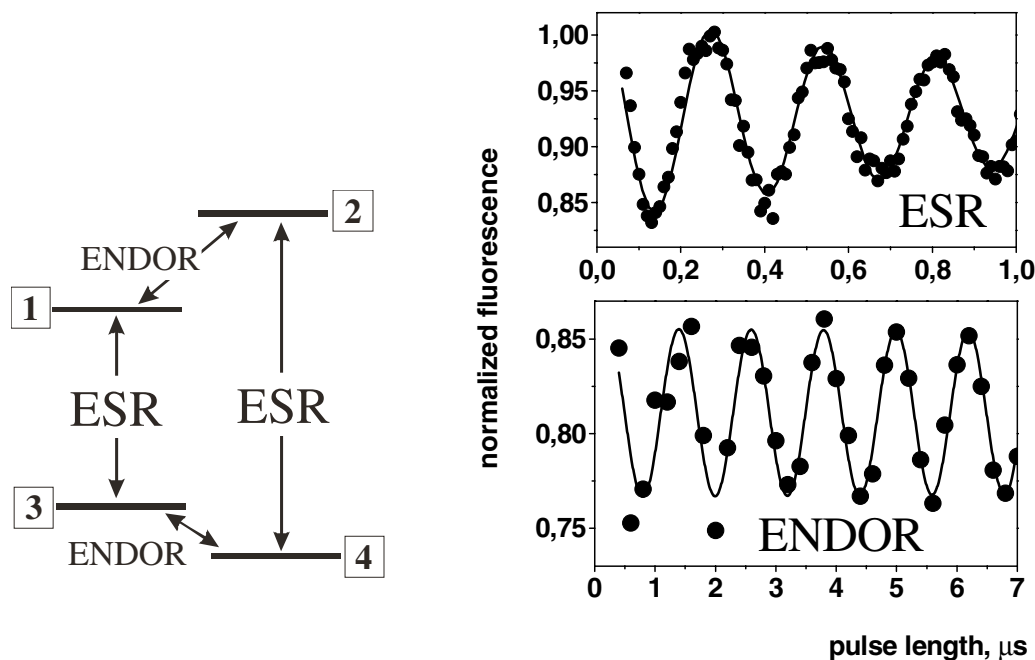


**Fig. 13** Energy level scheme and Rabi nutations of a single NV electron spin coupled to a single  $^{13}\text{C}$  spin. The left part of the figure shows the relevant spin levels for the coupled electron-nuclear spin system. The allowed electron spin resonance (ESR) and nuclear magnetic resonance (NMR) transitions are shown in the figure. The right part of the figure shows Rabi nutations of an electron spin (upper trace) and nuclear spin (lower trace).

( $T_2 = 2 \mu\text{s}$  in the present case) this is not the case here. Instead the inversion of the spin is not complete and coherences (no diagonal elements) are created. The behaviour can be reproduced when a full density matrix treatment of the pulse acting on the 4 level system is carried out as shown on the right side of Fig. 14.

## 8 Controlled generation of defect centres

The nitrogen vacancy centre in diamond is traditionally observed in radiation damaged nitrogen rich diamond. The centre is formed from the vacancy after annealing with temperatures larger than  $600^\circ\text{C}$ . The vacancy gets mobile and forms a stable NV complex under these conditions. Well controlled generation of NV colour centres has been achieved by this approach [60]. Electron (400 keV) and Ga (30 keV) ion beams were used to generate localized areas of NV centres in Ib diamond. For 30 keV Ga ions the nominal penetration depth of ions inside the material is 15 nm. Patterns of NV centres have been generated with some ten thousand Ga ions used per irradiated dot. From the experiments the diffusion constant of vacancies in diamond has been determined to be  $D = 1.1 \frac{\text{nm}^2}{\text{s}}$ . The activation energy for vacancy

diffusion is calculated to be 2.4 eV. Electrons with 400 keV penetrate some  $\mu\text{m}$  inside the diamond sample. At high irradiation dose an increased generation of  $\text{NV}^0$  centres was observed. For a localized generation of NV defects these approaches do have the disadvantage of the relative high diffusion constant of the vacancy plus the large “natural” abundance of nitrogen. For generating NV defects with large spin dephasing times for example it would be preferential to implant defects into nitrogen free samples. This is possible by implanting nitrogen directly into type IIa diamonds. In a first attempt 2 MeV nitrogen

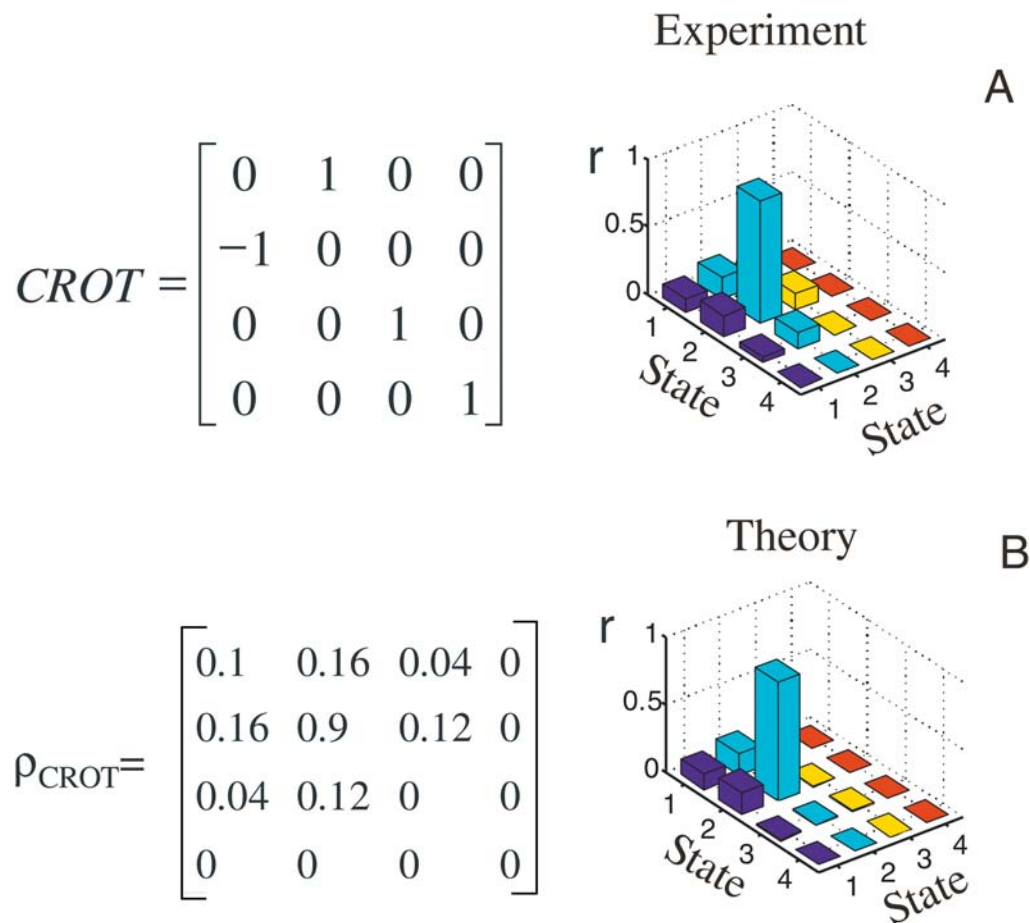


**Fig. 14** (online colour at: [www.pss-a.com](http://www.pss-a.com)) Schematic representation of the experimental and theoretical outcome of a CROT gate on a coupled singlet electron spin nuclear spin system. The upper left part shows the matrix representing the unitary transformation CROT. The other figure represents the density matrix of the two spin systems after the CROT gate, in a graphical representation. Part B represents a numerical calculation of the experimental results.

atoms have been implanted into type IIa diamond substrates [61] (Fig. 15a). STRIM calculations suggest that the ions should be found 1  $\mu\text{m}$  below the surface. The lateral scattering in the end position of the nitrogen (straggling) should be 0.5  $\mu\text{m}$ . With a displacement energy of 55 eV for carbon and a density of 3.5  $\text{g}/\text{cm}^3$  about 200 vacancies should be produced during a single nitrogen implantation. Indeed the optical spectra of the implantation areas do show mostly fluorescence emission from neutral vacancies prior to annealing. After annealing, fluorescence from mostly NV centres is found. In these studies the number of nitrogens implanted per spot has been decreased gradually. Single centre emission was observed when on average two ions are implanted in a single spot (see Fig. 15b). It is however difficult to ensure that the generated NV indeed is made from the nitrogen implanted and not from an abundant one. Even with a nitrogen concentration below 0.1 ppm there would be 30 native nitrogen atoms in a spherical volume of 150 nm surrounding the end range where the Bragg peak in the stopping power creates the maximum concentration of vacancies. Hence there is a considerable chance in Fig. 15 that the NV fluorescence does not stem from an implanted nitrogen. To be able to separate implanted from impurity ni-

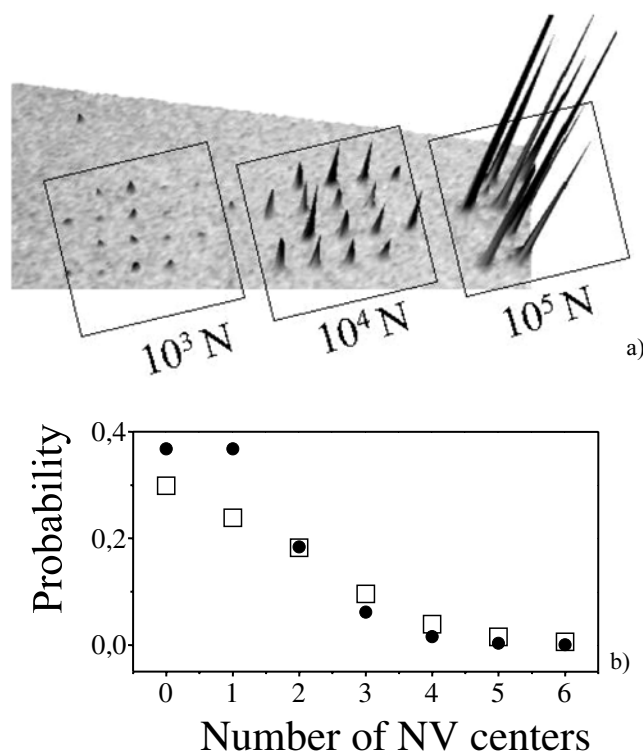


**Fig. 15** Fluorescence image of a type IIa diamond irradiated with a  $\text{N}^+$  ion micro beam at different nitrogen dosages (a). (b) Probability to generate the given number of defects for a deposition of two nitrogen ions per spot. Open squares are measured data and filled circles are calculated values.

trogen,  $^{15}\text{N}$  has been used as an implantation ion.  $^{15}\text{N}$  has a nuclear spin angular momentum  $I = \frac{1}{2}$  with a characteristically different ODMR spectrum from  $^{14}\text{N}$  (see Fig. 10a) [62]. Experimentally 14 keV  $^{15}\text{N}_2^+$  ions have been implanted. From a comparison of the number  $^{15}\text{NV}$  defect centres to the number of implanted  $^{15}\text{N}$  the efficiency of NV defect generation has been calculated. Under the conditions employed in the experiment this efficiency was about 2.5%. It should be noted however, that a 14 keV implantation of  $\text{N}_2$  results in a penetration depth of only a few nm. This close proximity to the surface might lead to a loss of vacancies due to diffusion to the surface. In any case the experiments demonstrate that single defects can be generated close to a diamond surface.

## 9 Fluorescent defects in diamond nanocrystals

Due to its chemical inertness and biocompatibility diamond is a material of choice in biosensing. In the recent future, progresses in cell biology on the other hand have caused an increased demand in biolabels. Here important figure of merits are biochemical variability, biocompatibility and photostability. Especially the latter two points are fulfilled ideally in diamond. In order to allow for labelling in cell biological applications, diamond nanocrystals have to be used. Diamond nanocrystals can be either made by milling bulk diamond or via detonation growth. Both forms are available commercially. While stable NV fluorescence has been demonstrated in milled diamond nanocrystals, no such observations have been published up to now for explosion grown diamond. Fluorescence from NV centres has been detected in diamond nanocrystals with sizes down to 20 nm. In a recent report the biocompatibility of diamond nanocrystals was investigated [63]. Upon addition of diamond nanocrystals in the buffer medium of a cell culture no deterioration in cell survival was detected. Most notably the endocytosis of diamond



nanocrystals in cells has been seen. However it should be noted that in other studies an increased cell death rate was measured [64, 65].

## 10 Outlook

The application of colour centres in diamond will rely on progresses in quality control of diamond material and the ability of precise generation of defects. In the first area it will be important to fabricate diamond with controlled impurity content. This refers to paramagnetic impurities like nitrogen but also to  $^{13}\text{C}$ . In addition it will be important to fabricate two- and three dimensional diamond structures with photoactive defect centres inside. One aim would be to build optical resonators out of diamond and to detect the coupling between the cavity mode and colour centres implanted in the diamond, similar to what has been shown for quantum dots. This not only requires structuring and material growth but also controlled defect implantation. Currently the precision of nitrogen implantation is limited by the quality of the ion beam optics and the ion source. A substantial improvement might be the implantation through metal nano apertures like it has been shown for the implantation of phosphorus in silicon. Here lateral position accuracies on the order of 10 nm might be achieved using currently available technology. For photonics applications, e.g. positioning of defects inside cavities or wave guides this might be sufficient. However, for coupling of defects via their magnetic dipole interaction a further improvement is necessary. Here accuracies down to 2 nm might be necessary. Also for charge transport based read out in structures like single electron transistors, a positioning accuracy on this order of magnitude might be essential. Extraction of nitrogen ions from traps is a promising approach. In a recent proposal nitrogen ions are sympathetically cooled down to some mK in a radio frequency trap. Subsequently they are extracted from the trap and imaged onto a diamond sample. This would result in a sub-nm resolution. Achieving such an accuracy in single defect centre positioning would open the door to new device fabrication technology which might be of fundamental impact to future quantum technology.

**Acknowledgements** The work has been supported by the European Commission (via integrated project “Quantum applications”), ARO, DFG (via SFB/TR 21 and graduate college “Magnetische Resonanz”), and the Landestiftung BW (via the programme “Atomoptik”).

## References

- [1] P. W. Shor, in: Proc. 37<sup>th</sup> Symp. on the Foundation of Computer Science (IEEE Press, Los Alamitos, California, 1996), pp. 56–65.
- [2] M. A. Nielsen and I. L. Chung, Quantum Computation and Quantum Information (Cambridge University Press, Cambridge UK, 2000).
- [3] D. Deutsch, Quantum-Theory, the Church–Turing Principle and the Universal Quantum Computer, Proc. R. Soc. Lond. A, Math. Phys. Eng. Sci. **400**(1818), 97–117 (1985).
- [4] G. Davies, S. C. Lawson et al., Vacancy-Related Centres in Diamond, Phys. Rev. B **46**(20), 13157–13170 (1992).
- [5] H. Haffner, W. Hansel et al., Scalable multiparticle entanglement of trapped ions, Nature **438**(7068), 643–646 (2005).
- [6] H. Haffner, F. Schmidt-Kaler et al., Robust entanglement, Appl. Phys. B, Lasers Opt. **81**(2–3), 151–153 (2005).
- [7] M. Riebe, H. Haffner et al., Deterministic quantum teleportation with atoms, Nature **429**(6993), 734–737 (2004).
- [8] M. D. Barrett, J. Chiaverini et al., Deterministic quantum teleportation of atomic qubits, Nature **429**(6993), 737–739 (2004).
- [9] S. Gulde, M. Riebe et al., Implementation of the Deutsch–Jozsa algorithm on an ion-trap quantum computer, Nature **421**(6918), 48–50 (2003).
- [10] D. J. Wineland, M. Barrett et al., Quantum information processing with trapped ions, Philos. Trans. R. Soc. Lond. A, Math. Phys. Eng. Sci. **361**(1808), 1349–1361 (2003).
- [11] J. Q. You and F. Nori, Superconducting circuits and quantum information, Phys. Today **58**(11), 42–47 (2005).

- [12] X. Q. Li, Y. W. Wu et al., An all-optical quantum gate in a semiconductor quantum dot, *Science* **301**(5634), 809–811 (2003).
- [13] J. R. Petta, A. C. Johnson et al., Coherent manipulation of coupled electron spins in semiconductor quantum dots, *Science* **309**(5744), 2180–2184 (2005).
- [14] F. H. L. Koppens, J. A. Folk et al., Control and detection of singlet-triplet mixing in a random nuclear field, *Science* **309**(5739), 1346–1350 (2005).
- [15] R. Hanson, L. H. W. van Beveren et al., Single-shot readout of electron spin states in a quantum dot using spin-dependent tunnel rates, *Phys. Rev. Lett.* **94**(19), 196802 (2005).
- [16] B. E. Kane, Silicon-based quantum computation, *Fortschr. Phys. – Prog. Phys.* **48**(9–11), 1023–1041 (2000).
- [17] G. Davies, Properties and growth of diamond (INSPEC, The Institution of Electrical Engineers, EMIS Data Review Series, London, 1994).
- [18] G. Davies and M. F. Hamer, Optical Studies of 1.945 eV vibronic band in diamond, *Proc. R. Soc. Lond. A, Math. Phys. Eng. Sci.* **348**(1653), 285–298 (1976).
- [19] J. Loubser and J. A. Vanwyk, Electron–spin resonance in study of diamond, *Rep. Prog. Phys.* **41**(8), 1201–1248 (1978).
- [20] Y. Mita, Change of absorption spectra in type-Ib diamond with heavy neutron irradiation, *Phys. Rev. B* **53**(17), 11360–11364 (1996).
- [21] A. T. Collins, M. F. Thomaz et al., Luminescence decay time of the 1.945 eV centre in type Ib diamond, *J. Phys. C, Solid State Phys.* **16**(11), 2177–2181 (1983).
- [22] R. T. Harley, M. J. Henderson et al., Persistent spectral hole burning of color-centres in diamond, *J. Phys. C, Solid State Phys.* **17**(8), L233–L236 (1984).
- [23] D. Redman, S. Brown et al., Origin of persistent hole burning of N–V centres in diamond, *J. Opt. Soc. Am. B, Opt. Phys.* **9**(5), 768–774 (1992).
- [24] A. Lenef, S. W. Brown et al., Electronic structure of the N–V centre in diamond: Experiments, *Phys. Rev. B* **53**(20), 13427–13440 (1996).
- [25] A. Lenef and S. C. Rand, Electronic structure of the N–V centre in diamond: Theory, *Phys. Rev. B* **53**(20), 13441–13455 (1996).
- [26] D. A. Redman, S. Brown et al., Spin dynamics and electronic states of N–V centres in diamond by EPR and 4-wave-mixing spectroscopy, *Phys. Rev. Lett.* **67**(24), 3420–3423 (1991).
- [27] J. Harrison, M. J. Sellars et al., Optical spin polarisation of the N–V centre in diamond, *J. Lumin.* **107**(1–4), 245–248 (2004).
- [28] N. R. S. Reddy, N. B. Manson et al., 2-Laser spectral hole burning in a color centre in diamond, *J. Lumin.* **38**(1–6), 46–47 (1987).
- [29] P. R. Hemmer, A. V. Turukhin et al., Raman-excited spin coherences in nitrogen-vacancy color centres in diamond, *Opt. Lett.* **26**(6), 361–363 (2001).
- [30] A. P. Nizovtsev, S. Y. Kilin et al., Spin-selective low temperature spectroscopy on single molecules with a triplet-triplet optical transition: Application to the NV defect centre in diamond, *Opt. Spectrosc.* **94**(6), 848–858 (2003).
- [31] A. P. Nizovtsev, S. Y. Kilin et al., NV centres in diamond: spin-selective photokinetics, optical ground-state spin alignment and hole burning, *Physica B, Condens. Matter* **340**, 106–110 (2003).
- [32] L. S. Zhang, X. M. Feng et al., Coherent transient in dressed-state and transient spectra of Autler–Townes doublet, *Phys. Rev. A* **70**(6), 063404 (2004).
- [33] A. S. M. Windsor, C. J. Wei et al., Experimental studies of a strongly driven Rabi transition, *Phys. Rev. Lett.* **80**(14), 3045–3048 (1998).
- [34] S. A. Holmstrom, C. J. Wei et al., Spin echo at the Rabi frequency in solids, *Phys. Rev. Lett.* **78**(2), 302–305 (1997).
- [35] N. B. Manson, C. J. Wei et al., Response of a two-level system driven by two strong fields, *Phys. Rev. Lett.* **76**(21), 3943–3946 (1996).
- [36] C. J. Wei, N. B. Manson et al., Dressed state nutation and dynamic Stark switching, *Phys. Rev. Lett.* **74**(7), 1083–1086 (1995).
- [37] M. Glasbeek and E. Vanoort, Coherent transients of the N–V centre in diamond, *Radiat. Eff. Defects Solids* **119**, 301–306 (1991).
- [38] E. Vanoort and M. Glasbeek, Electric-field-induced modulation of spin echoes of N–V centres in diamond, *Chem. Phys. Lett.* **168**(6), 529–532 (1990).

- [39] E. Vanoort, N. B. Manson et al., Optically detected spin coherence of the diamond N–V centre in its triplet ground-state, *J. Phys. C, Solid State Phys.* **21**(23), 4385–4391 (1988).
- [40] S. C. Rand, A. Lenef et al., Zeeman coherence and quantum beats in ultrafast photon-echoes of N–V centres in diamond, *J. Lumin.* **60**(1), 739–741 (1994).
- [41] D. Redman, Q. Shu et al., 2-Beam coupling by nitrogen-vacancy centres in diamond, *Opt. Lett.* **17**(3), 175–177 (1992).
- [42] X. F. He, N. B. Manson et al., Paramagnetic-resonance of photoexcited N–V defects in diamond, 1. level anticrossing in the (3)g ground-state, *Phys. Rev. B* **47**(14), 8809–8815 (1993).
- [43] X. F. He, N. B. Manson et al., Paramagnetic-resonance of photoexcited N–V defects in diamond. 2. Hyperfine interaction with the N-14 nucleus, *Phys. Rev. B* **47**(14), 8816–8822 (1993).
- [44] C. J. Wei and N. B. Manson, Observation of electromagnetically induced transparency within an electron spin resonance transition, *J. Opt. B, Quantum Semiclass. Opt.* **1**(4), 464–468 (1999).
- [45] J. Isoya, H. Kanda et al., Fourier-transform and continuous-wave EPR studies of nickel in synthetic diamond – site and spin multiplicity, *Phys. Rev. B* **41**(7), 3905–3913 (1990).
- [46] V. A. Nadolinny, A. P. Yelisseyev et al., A study of C-13 hyperfine structure in the EPR of nickel-nitrogen-containing centres in diamond and correlation with their optical properties, *J. Phys.: Condens. Matter* **11**(38), 7357–7376 (1999).
- [47] T. Gaebel, I. Popa et al., Stable single-photon source in the near infrared, *New J. Phys.* **6**, 98 (2004).
- [48] M. Orrit, Single-molecule spectroscopy: The road ahead, *J. Chem. Phys.* **117**(24), 10938–10946 (2002).
- [49] A. Gruber, A. Drabenstedt et al., Scanning confocal optical microscopy and magnetic resonance on single defect centres, *Science* **276**(5321), 1012–1014 (1997).
- [50] C. Kurtsiefer, S. Mayer et al., Stable solid-state source of single photons, *Phys. Rev. Lett.* **85**(2), 290–293 (2000).
- [51] A. Beveratos, R. Brouri et al., Nonclassical radiation from diamond nanocrystals, *Phys. Rev. A* **64**(6), 061802 (2001).
- [52] R. Brouri, A. Beveratos et al., Photon antibunching in the fluorescence of individual color centres in diamond, *Opt. Lett.* **25**(17), 1294–1296 (2000).
- [53] R. Alleaume, F. Treussart et al., Experimental open-air quantum key distribution with a single-photon source, *New J. Phys.* **6**, 92 (2004).
- [54] A. Mainwood and A. M. Stoneham, The vacancy ( $V-0$ ,  $V+$ ,  $V-$ ) in diamond: The challenge of the excited states and the GR2–GR8 lines, in: *Proceedings of the 13th International Conference on Defects in Insulating Materials – ICDIM 96*, Vol. 239-2 (1997).
- [55] T. Gaebel, C. Wittmann, I. Popa, F. Jelezko, J. Rabeau, A. Greentree, S. Prawer, E. Trajkov, P. R. Hemmer, and J. Wrachtrup, Photochromism in single nitrogen-vacancy defects in diamond, *Appl. Phys. B, Laser Opt.*, DOI:10.1007/s00340-005-2056-2 (2005).
- [56] I. Popa, T. Gaebel et al., Energy levels and decoherence properties of single electron and nuclear spins in a defect centre in diamond, *Phys. Rev. B* **70**(20), 201203 (2004).
- [57] F. Jelezko, T. Gaebel et al., Observation of coherent oscillation of a single nuclear spin and realization of a two-qubit conditional quantum gate, *Phys. Rev. Lett.* **93**(13), 130501 (2004).
- [58] T. A. Kennedy, J. S. Colton et al., Long coherence times at 300 K for nitrogen-vacancy centre spins in diamond grown by chemical vapor deposition, *Appl. Phys. Lett.* **83**(20), 4190–4192 (2003).
- [59] F. Jelezko, T. Gaebel et al., Observation of coherent oscillations in a single electron spin, *Phys. Rev. Lett.* **92**(7), 076401 (2004).
- [60] J. Martin, R. Wannemacher, J. Teichert, L. Bischoff, and B. Kohler, Generation and detection of fluorescent color centres in diamond with submicron resolution, *Appl. Phys. Lett.* **20**, 3096–3098 (1996).
- [61] J. Meijer, B. Burchard, M. Domhan, C. Wittmann, T. Gaebel, I. Popa, F. Jelezko, and J. Wrachtrup, Generation of single colour centres by focussed nitrogen implantation, *cond-mat/0505063* (2006).
- [62] J. R. P. Rabeau, G. Tamanyan, D. N. Jamieson, S. Prawer, F. Jelezko, T. Gaebel, I. Popa, M. Domhan, and J. Wrachtrup, Implantation of labelled single nitrogen vacancy defect centre in diamond using  $^{15}\text{N}$ , *cond-mat/0511722* (2006).
- [63] S.-J. Yu, M.-W. Kang, H.-C. Chang, K.-M. Chen, and Y.-C. Yu, Bright fluorescent nanodiamonds: no photobleaching and low cytotoxicity, *J. Am. Chem. Soc.* **127**, 17604/17605 (2005).
- [64] A. P. Puzyr, D. A. Neshumayev et al., Destruction of human blood cells in interaction with detonation nanodiamonds in experiments in vitro, *Diam. Relat. Mater.* **13**(11/12), 2020–2023 (2004).
- [65] V. S. Bondar' and A. P. Puzyr', Nanodiamonds for biological investigations, *Phys. Solid State* **46**(4), 716–719 (2004).